Available online at www.sciencedirect.com
ScienceDirect
Superlattices and Microstructures 43 (2008) 1–23
Superlattices and Microstructures
www.elsevier.com/locate/superlattices

Review

InGaN: An overview of the growth kinetics, physical properties and emission mechanisms

F.K. Yam*, Z. Hassan

School of Physics, Universiti Sains Malaysia, 11800 Penang, Malaysia

Received 5 March 2007; received in revised form 10 May 2007; accepted 10 May 2007
Available online 13 June 2007

Abstract

This article reviews the fundamental properties of InGaN materials. The growth kinetics associated with the growth parameters, such as growth temperatures, V/III ratios, and growth rates which influence the quality of the InGaN epilayers, are briefly described. An overview of the properties of the InGaN alloys, such as the optical, structural and electrical characteristics, is presented. The design and fabrication of novel optoelectronic device structures require an accurate knowledge of the band gap as a function of alloy composition; therefore, attention is paid to Vegard's law and the bowing parameter; in addition, the major factors leading to the uncertainties of the bowing parameter of InGaN are addressed. Apart from that, the determination of indium composition by X-ray diffraction (XRD) using different assumptions and various equations are summarized. The erroneous measurements of the indium composition by using this technique are also described. Finally, different emission mechanisms of the strained InGaN quantum wells proposed by different groups of researchers are also discussed.

Keywords: InGaN; Growth kinetics; Physical properties; Bowing parameter; Emission mechanisms

Contents

1. Introduction 2
2. The growth kinetics of InGaN 3
3. The properties of InGaN 5
   3.1. Optical properties 5
   3.2. Structural properties 8

* Corresponding author. Tel.: +60 4 6533673; fax: +60 4 6579150.
E-mail address: yamfk@yahoo.com (F.K. Yam).

0749-6036/$ - see front matter © 2007 Elsevier Ltd. All rights reserved.
doi:10.1016/j.spmi.2007.05.001

3.3. Electrical properties 10
4. Vegard's law and bowing 11
4.1. Factors contributing to the inaccuracy of bowing parameter 12
5. Determination of indium composition by XRD 13
6. Indium segregation and piezoelectricity 17
7. Conclusions 18
Acknowledgements 19
References 19

1. Introduction

The nitride semiconductors, such as gallium nitride (GaN) and related alloys, have received enormous attention because of their broad range of practical applications. The nitride semiconductors form a continuous alloy system with direct band gaps, ranging from about 0.7 (InN) to 6.2 eV (AlN) with 3.4 eV for GaN. Band gaps adjustable from 0.7 to 6.2 eV can be achieved by suitable alloy combinations in the InGaN and AlGaN systems from which heterojunctions can be fabricated.

Among the ternary compounds of III-nitride materials, InGaN has drawn a great deal of attention. GaN and Ga-rich InGaN have been considered as the most important and indispensable materials used for the fabrication of light emitters which are active in entire visible and part of the near UV spectral regions. Despite recent significant progress in InGaN technology, however, the fundamental physics related to the InGaN materials has not been well developed. Some of the physical and chemical properties are still estimated based on the two binary compounds, GaN and InN: for instance, the band gap, lattice parameters, elastic constants, effective electron mass and others. In addition, the band gap energy of InN has been experimentally shown to be smaller than 1.0 eV [1–7]; however, there is still much debate on the correct fundamental band gap. Several groups [8–10] even supported the old 1.9 eV InN band gap by presenting their experimental data to substantiate their claim. These fundamental problems have led to uncertainties in computing the optical, structural and electrical parameters of the InGaN, and eventually result in the inaccuracy of the technical data in the literature. To date, the fundamental properties of GaN are relatively well established, and many excellent review papers can be found in the literature [11–18]. In contrast, the study of InN is still in the early stage, in which most of the fundamental properties are not well documented. This further complicates the study of InGaN. However, some of the physical parameters and properties could be obtained from review papers published recently [5,12,19–21].

It is well known that the optical, structural and electrical characteristics of InGaN alloys can be significantly affected by the growth conditions. The slight adjustment of the growth parameters could lead to a large variation in the quality of the InGaN thin films; therefore an understanding of the growth kinetics of InGaN is of great importance, and this, eventually, may help to develop and fabricate better quality InGaN films by optimizing the growth parameters.

Designing and fabricating novel optoelectronic device structures so that their optical emission characteristics can be tailored require not only an accurate knowledge of the band gap as a function of alloy composition but also an in-depth understanding of the fundamental properties of the InGaN materials. However, the presence of some technical difficulties, for instance, the difficulty in growing high-quality InGaN alloys, especially alloys with high InN molar fraction, as well as the inaccuracy and uncertainties in determining the indium composition, is among the

problems which could have affected the fabrication of high-performance optoelectronic devices with the desired optical properties.

Although InGaN material has long been used as an active material for the fabrication of optoelectronic devices, the emission mechanism still remains an enigma: different models of emission mechanisms have been proposed by different groups. In addition, in low-temperature growth, two separate phases of material could be present within the same quantum well (QW); this further complicates the emission dynamics in the material.

This article reviews and summarizes the growth kinetics, fundamental properties, Vegard's law and bowing parameter, and determination of indium composition by X-ray diffraction (XRD), as well as the emission mechanisms of InGaN materials.

2. The growth kinetics of InGaN

It is a challenging task to grow InGaN materials. The difficulties in growing high-quality InGaN materials can be attributed to a number of problems: for instance, the large difference in interatomic spacing between InN and GaN results in a solid phase miscibility gap [22,23] and the relatively high vapor pressure of InN as compared to the vapor pressure of GaN leading to low indium incorporation in the InGaN alloy [24]; in addition, the difference in formation enthalpies for InN and GaN causes a strong indium surface segregation on the growth front [25]. These problems, however, can be minimized by optimizing the growth parameters, such as the use of relatively low growth temperatures, high V/III flux ratio, low growth rate and low growth pressure.

The investigation of different growth parameters on indium incorporation is essential during the growth of InGaN: it provides valuable information on the growth kinetics. Piner et al. [26] reported the growth of InGaN by atmospheric pressure metal organic chemical vapor deposition (AP-MOCVD): they pointed out that as the growth temperature is reduced, desorption of the indium from the surface is substantially reduced; on the other hand, the cracking of ammonia will be less efficient at low temperatures, and this leads to a reduced growth rate which could cause reduction in indium incorporation into the film. Both of these phenomena result in an increase in the density of indium atoms diffusing across the film surface and increase the probability of forming indium clusters. Once these clusters reach a critical size, they become thermodynamically stable and can grow bigger. These indium droplets will act as sinks for available indium surface atoms, thus competing with, and in some cases dominating, the process of indium incorporation in the InGaN film. Typically the amount of indium droplets increases substantially with the reduction of growth temperature.

Large V/III ratios were found to be able to suppress the indium segregation during growth of InGaN [27,28]. Van der Stricht et al. [27] reported that, at growth temperatures below 750 °C, the surface was covered with metal droplets, and the film showed a grey colour to the naked eye. The amount of indium on the surface decreases with increasing ammonia flow; this is due to the increased availability of nitrogen bonding sites for the indium, as a result of the increased amount of nitrogen radicals from ammonia [26]. The growth of In-based structures exhibits different growth characteristics than bulk In-based nitrides. Thin InGaN heterostructures have higher InN% and no indium metal on the surface compared to bulk grown InGaN. This can be attributed to a critical time at growth temperature required to form the critical indium metal nucleus size. Below the critical time, no formation of indium droplet is observed, but instead there is a high density of indium atoms on the surface. These atoms will either desorb or incorporate into the film once the top layer growth has begun forming a high InN% film. However, when the critical time is exceeded, indium droplets will be formed which could have deleterious effects

on the structure. Moreover, the morphology of InGaN also could be influenced by the amount of NH_3 on the growing surface. The transition from island nucleation mode to step-flow mode has been reported with the increase of NH_3 flow rate; this behaviour could be attributed to the reduction in the energy barrier to adatom incorporation at the step-edges [29].

The indium incorporation in bulk InGaN films was found to be affected not only by growth temperature but the growth rate and growth pressure as well. During growth of the InGaN alloys, the evaporation of indium species from the surface will be suppressed at lower temperatures and higher growth rates as the indium species become trapped by the growing layer [30,31]. The incorporation of indium will strongly increase while decreasing growth temperatures from 850 to 500 °C; however, indium droplets, phase separation and composition inhomogeneity are observed in the InGaN films with a high indium composition, and these lead to lower quality material which could be attributed to the low surface mobility of the adatoms [32,33]. However, at growth temperatures below 760 °C, high-quality InGaN could be obtained by reducing the growth rate [31], since lower growth rate allows adatoms on the surface to have longer time to arrive at two-dimensional step edges of growth front and thereby enhances optical and crystal quality [34]. Kim et al. [35] studied the effect of growth pressure on indium incorporation: they found that indium incorporation in the InGaN film was drastically increased with decreasing the growth pressure from 250 to 150 Torr; a similar finding was also reported by Oliver et al. [29]. The enhanced mass transportation of precursor gases through the boundary layer on the substrate in the MOCVD system was proposed to be responsible for this behaviour; however, the decrease of growth pressure was accompanied by a large red-shift and broadening of the PL spectra, and this result indicated the degradation of the optical properties of the InGaN films which could be due to the inhomogeneous distribution of indium in the InGaN alloys.

At present, MOCVD is the leading growth technique for the fabrication of most of the GaN-based structures and optoelectronic devices; however, molecular beam epitaxy (MBE) is fast emerging as an alternative growth technique, especially for the growth of high-quality single-crystalline InN [21,36]. The growth of III-nitride materials by MBE evolves with the introduction of efficient nitrogen sources and a homoepitaxial growth approach. In particular, radio-frequency (rf) MBE has a number of advantages over the MOCVD technique: for instance, the hydrogen-free growth environment allows p-type doping of GaN-based materials without a post-growth heat treatment, and the consumption of source materials is significantly reduced. In addition, the atomic nitrogen species produced from an rf source for incorporation into the growing front are independent of the substrate temperature [37].

Usually, the growth of III-nitride semiconductors by MBE is carried out under conditions far from thermodynamic equilibrium and is mainly controlled by the kinetics of the surface processes which takes place when the impinging species react with the outermost atomic layers; this is different from MOCVD, in which the growth is conducted under near thermodynamic equilibrium conditions and it is governed by diffusion processes [38].

The characteristics of indium incorporation during InGaN growth by MBE are found to be quite similar to MOCVD in certain aspects. When the substrate temperature is increased, the indium incorporation decreases [39–41]; however, when the temperature and N_2 flux are maintained constant, and both In and Ga fluxes are increased while their ratio is kept constant, the indium incorporation is found to be increased at low metal flux, but it decreases at high metal flux. Chen et al. [39] pointed out that when both In and Ga fluxes are increased, the additional Ga atoms will compete to go into the bulk: since there is strong indium surface segregation, most of the additional Ga atoms will go into the bulk and displace the indium atoms; eventually the indium incorporation will decrease.

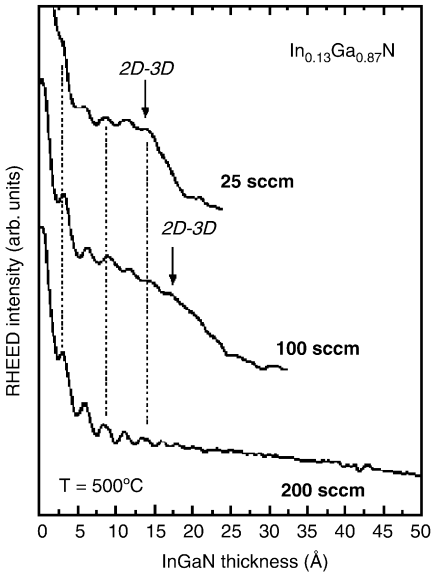

Fig. 1. RHEED intensity oscillations showing the delay of the 2D–3D growth mode transition when the NH_3 flux is increased. (After Ref. [42]. Reproduced from N. Grandjean, B. Damilano, J. Massies, J. Phys.: Condens. Matter 13 (2001) 6945 with permission from IOP).

Grandjean et al. [42] studied InGaN/GaN quantum well (QW) samples grown by MBE using ammonia as the N-precursor. The indium composition will increase when the V/III ratio is increased by supplying larger NH_3 flux. The change of growth mode was observed and monitored by reflection high energy electron diffraction (RHEED) for different NH_3 flow rates. Under low NH_3 flow (50 sccm), a two-dimensional to three-dimensional (2D–3D) transition growth mode after a few monolayers (ML) was found; however, the 2D–3D growth mode transition was no longer observed with larger NH_3 flow (200 sccm). RHEED intensity oscillations showing the delay of the 2D–3D growth mode transition when NH_3 flux is increased are illustrated in Fig. 1. The surfactant effects of hydrogen and/or NH_x radicals were suggested to be responsible for the change of growth mode, and the suppression of the 2D–3D growth mode transition could be due to an increase of the surface free energy of the (0001) plane induced by the presence of hydrogen produced by the decomposition of NH_3.

3. The properties of InGaN

3.1. Optical properties

The optical properties of InGaN can be influenced by a number of factors: for instance, the indium molar fraction, growth rate, and growth temperatures as well as the thickness of the InGaN. For MOCVD-grown InGaN alloys, the incorporation of indium is found to be increased with decreasing temperature [26,43–46]. For samples grown at high temperature ($T_g \geq 750$ °C), prominent near band edge emission is observed, whereas for samples grown at low temperature ($T_g \leq 700$ °C), a deep level or impurity transition is found to be dominant [43]. At high growth temperatures, the ratio of band edge to deep level emission is found to be increased [27]. Fig. 2 illustrates a typical photoluminescence (PL) spectrum of InGaN samples grown at different

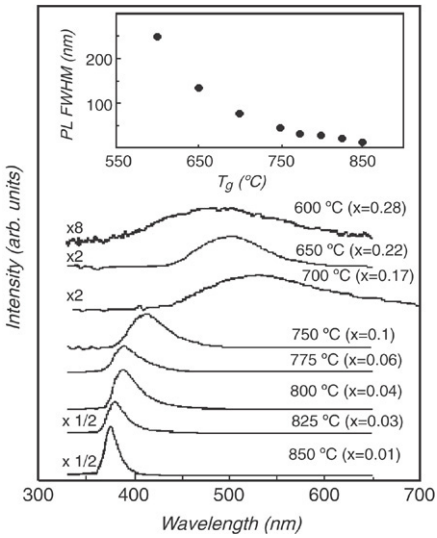

Fig. 2. PL spectra of InGaN samples grown at different temperatures showing strong BE emissions for $T_g \geq 750\,^{\circ}\mathrm{C}$ and dominant impurity transition for $T_g \leq 750\,^{\circ}\mathrm{C}$. (After Ref. [43]. Reprinted from H.-C. Lin, C.-K. Shu, J. Ou, Y.-C. Pan, W.-K. Chen, W.-H. Chen, M.-C. Lee, Growth temperature effects on $In_xGa_{1-x}N$ films studied by X-ray and photoluminescence, J. Crystal. Growth 189–190 (1998) 57 with permission from Elsevier).

temperatures for different indium composition. The PL spectra obtained normally shows that the band edge (BE) emission intensity decreased with increasing indium composition. On the other hand, the full width at half maximum (FWHM) of the BE peak is found to be increased with indium composition [26,43,44,47].

Growth rate is one of the important factors determining the optical properties and quality of the InGaN epilayers [30,31,33,34,48,49]. At higher growth rates, the incorporation of indium becomes higher; the low-temperature PL spectra of indium-rich InGaN were found to be dominated by a deep and broad emission band. The degradation of the optical quality of the indium-rich InGaN films with increased growth rate could be attributed to the reduction of the effective lateral mobility of the indium adatoms which leads to the formation of compositional fluctuation in the alloy [49]. On the other hand, Lee et al. [34] reported that for lower growth rate, higher PL intensity is observed, and more uniform PL wavelength is found from the micro PL wavelength mapping measurement; these imply that the optical quality is improved with decreasing inhomogeneity due to indium composition fluctuation.

Varying the indium mole fraction of InGaN layer between 0.2 and 0.7 was also used by Nakamura et al. [50] to change the peak wavelength from blue to yellow in InGaN single quantum well (SQW) LEDs. The peak wavelength and the FWHM of the typical electroluminescence (EL) spectra of blue, green and yellow SQW LEDs were reported to be 450 and 20 nm; 525 and 45 nm; 590 and 90 nm, respectively. The peak wavelength becomes longer, and the value of the FWHM of the EL spectra increases. The output power of green and yellow SQW LEDs is relatively small in comparison with that of blue SQW LEDs, probably due to poor crystal quality of the InGaN well layer, which has large lattice mismatch and difference in thermal expansion coefficient with barrier layers; however, the degradation of the emission quality could be also due to out-diffusion of the indium into the barrier layer. Generally, such out-diffusion becomes more serious in a sample with higher indium content [51]. More recently, Martin et al. [52] reported the

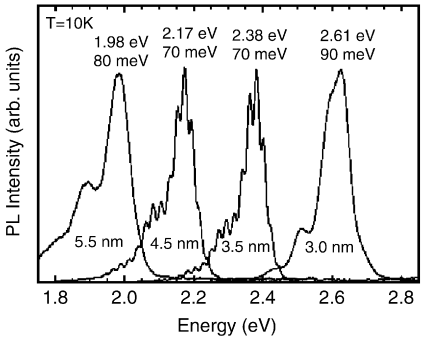

Fig. 3. PL spectra of $In_{0.2}Ga_{0.8}N$/GaN QWs of various thicknesses: 3, 3.5, 4.5 and 5.5 nm. (After Ref. [42]. Reproduced from N. Grandjean, B. Damilano, J. Massies, J. Phys.: Condens. Matter 13 (2001) 6945 with permission from IOP).

growth of InGaN SQWs with emission peaks in the blue, green, amber and red spectral regions. By manipulating the growth temperatures from 860 to 760 °C, PL peak wavelengths was found to be shifted progressively from 430 to 670 nm; similarly, the optical quality deteriorated with increasing indium content in the InGaN SQW.

Harris et al. [53] investigated the influence of ammonia, hydrogen, trimethylindium (TMIn) and total reactor flow rates on the optical properties of the $In_xGa_{1-x}N/In_yGa_{1-y}N$ MQWs. In their work, high ammonia flow rate, moderate hydrogen flow rate, high TMIn flow rate and low total reactor flow rate were found to give stronger PL intensity, as well as higher indium composition. These results contradict most of the published results found in the literature [43,50, 52,54], in which lower indium content is usually accompanied by stronger PL intensity.

Apart from these, some groups reported that varying the thickness or size of QWs or quantum dots (QDs) of InGaN (embedded in GaN or InGaN) could lead to the variation of the wavelengths [30,31,42,51,55–58]. With the decrease of thickness of InGaN, the blue-shift of the energy will be more pronounced. The shift of energy by changing the thickness or size of InGaN was attributed to the quantum-confined Stark effect induced by the presence of a huge piezoelectric field. Fig. 3 shows the low-temperature PL spectra of $In_{0.2}Ga_{0.8}N$/GaN with thickness varying from 3 to 5.5 nm; the PL energies are found to cover the whole visible spectra regions. Therefore, by combining two or more suitable wavelengths emitted from different thicknesses of these low-dimensional structures, white light could be generated. Researchers have been studying intensively the possibility of developing white LEDs by incorporating InGaN/GaN QWs with different thicknesses in the active region [42,55].

In addition to the thickness of InGaN QWs, the effect of the number of InGaN/GaN pairs also influences both the optical properties of the InGaN/GaN MQWs [59–63]. However, different results have been reported, and some of the findings are contradictory. Hurst et al. [63] investigated the variation of PL intensity and decay time as a function of temperature for a series of InGaN/GaN samples with different numbers of QWs. In their study, they found that the FWHM of the PL spectra at 6 K are 100, 92, 67, 55 and 53 meV for samples with 18, 10, 5, 3 and 2 QWs, respectively. The increased width of the PL spectra width for the samples with increasing number of QWs could be due to the changes in the average indium fraction in different wells; moreover, they also observed that PL intensity of all samples decreased as the temperature increased from 6 to 300 K, but with different rates. At 300 K, the sample with 2 QWs showed a reduction in intensity of 10,000 times, whereas 18 QWs sample exhibited a decrease

of intensity with a factor of 10 as compared to PL intensity measured at 6 K. Similarly, decay time was observed with increasing temperature with the rate of decrease more pronounced for the sample with fewer wells. On the other hand, Kim et al. [59] reported that the intensity of PL was decreased and the PL peak was red-shifted with increasing number of wells. The red-shift of the PL peaks could be attributed to the formation of In-rich precipitates in the MQWs, and the drop of peak intensity was mainly due to the deterioration of the interfacial structure [59]. Apart from that, Cheong et al. [60] reported that the shift of PL peak positions was independent of the number of wells. However, the emission intensity increased with increasing well number up to 6, and then decreased with further increasing of the well number.

The quantum barrier, usually referring to GaN, is another parameter which is found to play a relatively important role in determining the optical quality of InGaN/GaN MQWs [64–66]. Wen and Lee [64] studied the effect of barrier growth temperature on the properties of InGaN/GaN MQWs; they found that the increase of barrier growth temperature (700–950 °C) could reduce the well thickness and eventually lead to a blue-shift of the PL peak. They explained that the shift may be caused by the reduction of well width and strain arising due to vary the barrier growth temperature. The strain in the MQW subsequently will induce a piezoelectric field and therefore influence the effective band gap. Similar but more detailed work was also carried out and reported by Kim et al. [65]. In contrast, Kim et al. [66] studied the effect of barrier thickness on the optical properties of InGaN/GaN MQWs: the PL data obtained showed little trend with the barrier thickness; however, they claimed that the intensity and line-width of the PL were reduced and broadened with the increase of the GaN barrier thickness.

3.2. Structural properties

Similarly, the structural properties of the InGaN epilayers also play an important role in determining the performance of the light-emitting devices: for instance, the output power and external efficiency of the laser diodes. They are affected by the formation of stress-induced defects in the InGaN active layer which are commonly ascribed to the lattice and thermal expansion coefficients mismatch between InGaN and GaN epilayers [67]. It is well known that the crystalline microstructure quality is closely related to the growth parameters, and therefore they can influence the quality of the film significantly. However, the growth of high-quality InGaN epilayers by MOCVD has always been a difficult task due to the thermal instability of InN at temperatures above 500 °C and the low cracking efficiency of ammonia below 1000 °C. Growth at high temperature (800 °C) results in higher crystalline quality, however with low amount of InN in the alloy. On the other hand, higher InN content can be obtained at lower growth temperatures (500 °C), but at the expense of the crystalline quality [22]. Nakamura [68] grew InGaN films with indium composition, x, up to $x = 0.33$ at temperatures between 720 and 850 °C. When the growth temperature was reduced, the growth rate of InGaN films had to be decreased tremendously in order to obtain high-quality InGaN films. Obviously, there is a trade-off between the epilayer quality and the amount of InN incorporation into the alloy as the growth temperature is changed. Therefore, a compromise has been made for the growth temperature in the range of 500–850 °C. Fig. 4 shows the XRD measurements of InGaN grown at different temperatures. For a growth temperature of 750 °C and higher, a sub-micron size and hexagonal hillock patterned surface is observed, as revealed by scanning electron microscopy measurements [43].

Usually, for the growth of GaN at lower growth temperature, the adsorbed species would have lower surface mobility, which leads to poor surface morphology [33]. InGaN epilayers are

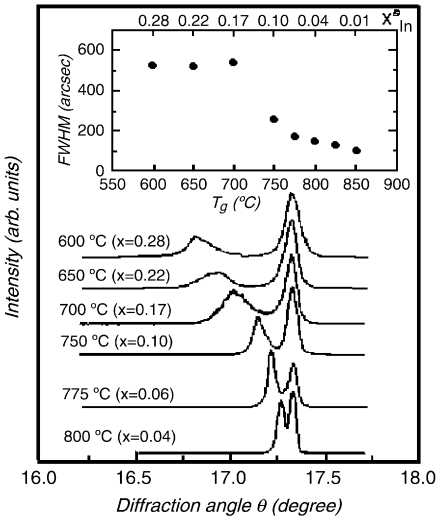

Fig. 4. X-ray θ–2θ diffraction pattern of InGaN grown at different temperatures, and the inset shows the FWHM of the (0002) InGaN peak. (After Ref. [43]. Reprinted from H.-C. Lin, C.-K. Shu, J. Ou, Y.-C. Pan, W.-K. Chen, W.-H. Chen, M.-C. Lee, Growth temperature effects on $In_xGa_{1-x}N$ films studied by X-ray and photoluminescence, J. Crystal. Growth 189–190 (1998) 57 with permission from Elsevier).

normally grown at much lower growth rates as compared to GaN epilayers. Lower growth rates are found to be able to minimize the formation of structural defects in the crystal [33,34,69]. Lee et al. [34] studied InGaN/InGaN QWs and reported that the threading dislocation density decreased remarkably by two orders of magnitude when the growth rate was reduced. On the other hand, the growth mechanism and the morphology of InGaN SQWs and bulk films are influenced by the dislocations. The threading dislocations of partial or pure screw character can send out successive turns of steps in the form of spirals leading to the growth of islands [70]. This spiral growth mode was found to be the dominant growth mechanism for InGaN SQWs grown under low trimethylgallium (TMG) flow rates by MOCVD, causing the formation of InGaN nanoscale islands [69]. In addition to the InGaN growth rate, the barrier growth rates also play a role in determining the structural quality of InGaN wells. Keller et al. [33] reported that at low GaN barrier growth rate, indium can desorb from the well layer, resulting in a lower average indium composition of the well and a higher compositional inhomogeneity.

Apart from this, the structural properties of InGaN/GaN MQWs could be significantly influenced by thickness of the GaN quantum barrier [66,71]. Kim [66] reported that with increasing thickness of the GaN (from 5.6 to 22.4 nm), the abruptness of the interface between InGaN/GaN layers deteriorated. The degradation of the InGaN/GaN MQWs was ascribed to the generation of defects induced by the strain accumulation in the MQWs. The structural quality of samples with different barrier thicknesses was reflected in the FWHM values of the zeroth-order satellite peaks determined from the XRD rocking curve. Similar work was also carried out by Shee et al. [71]; however, a contradictory finding was reported. In their work, GaN barrier thicknesses ranging from 4 to 15 nm were used. Their studies showed that both structural and optical quality were improved with larger barrier thickness.

The structural characteristics of InGaN also could be influenced by the application of growth interruption [72–77]. Several groups used the growth interruption time to fabricate nanoscale

InGaN self-assembled QDs. Ji et al. [73] demonstrated the growth of smaller size InGaN QDs when growth was interrupted for 12 s as compared to much larger QDs obtained without growth interruption. The samples prepared with growth interruption were also found to have stronger PL intensity accompanied with blue-shifting. On the other hand, Cheong et al. [75] claimed that the increase of the interruption time would lead to the reduction of the QD-like regions and well thickness, which were attributed to the indium re-evaporation. However, the density and the size of V-defects were constant with increasing interruption time. In contrast, Uchida et al. [76,77] reported that the size of the pits increased as the growth interruption time was increased. They pointed out that the formation of these pits could affect the indium incorporation into the InGaN QW and eventually led to the variation of growth rate when the subsequent QW structure was grown.

From the literature, high-performance InGaN-based optoelectronic devices have been exclusively grown by the MOCVD technique. In contrast, the MBE technique normally produced devices with lower efficiency, and it has long been viewed as an unsuitable technique for the fabrication of optoelectronic devices. Until quite recently, with the successful demonstration of MBE-grown InGaN laser diodes (LDs) [78–81], the performance of GaN-based optoelectronic devices fabricated by MBE are now considered to be comparable to those grown by MOCVD. However, it should be noted that these MBE-grown InGaN LDs were fabricated on GaN template substrates grown by MOCVD. The quality of InGaN epilayer grown by rf-MBE on Ga- or N-polarity GaN underlayers has been investigated intensively by Shen et al. [82–85]. In the studies, they found that the use of N-polarity GaN as an underlayer would lead to poor crystalline quality with a large FWHM value of the XRD (0002) InGaN diffraction peak and no PL emission in certain cases. In contrast, high-quality InGaN films were obtained when Ga-polarity GaN was used as the underlayer. Generally, GaN films grown by MBE always produce N-polarity [86,87]. Therefore, high-quality InGaN films are generally difficult to be grown by MBE as compared to MOCVD. A similar finding was also reported earlier by Prystawko et al. [88]: in their work, InGaN has been grown on different GaN substrates with N- and Ga-polarity by MOCVD; the InGaN film grown on Ga-polarity showed a much narrower PL peak with respect to the InGaN film grown on N-polarity.

3.3. Electrical properties

At present, most of the studies are focusing on optical and structural characteristics of InGaN; the electrical properties of this material are relatively less investigated. Kumakura et al. [89] studied the electrical properties of Mg-doped InGaN grown by MOCVD with indium mole fraction lower than 0.2. They demonstrated that the activation energy, E_A, of Mg acceptors in InGaN decreased with the increase of the indium content. As a result, Mg-doped InGaN ($x < 0.2$) with higher hole concentration at room temperature for higher In mole fraction was obtained. For other III-nitride semiconductors, the increase of E_A with the increase in energy gap has been reported by others [90,91], and this is also predicted by the effective mass theory [92, 93]. Chen et al. [94] investigated the hole concentration and mobilities of Mg-doped InGaN with different indium content (x from 0 to 0.4); they found that the measured hole concentration increased with the indium content, and this finding was in agreement with the study reported by Kumakura [89].

On the other hand, Nagatomo et al. [24] investigated the resistivity of $In_xGa_{1-x}N$ films grown on different substrate temperatures: in their studies, extremely high resistivities in the range of 10^9–10^{11} Ω cm were observed for those InGaN films grown below 620 °C; however, the

resistivities of InGaN films dropped drastically to the range of 10^{-2}–10^{-1} Ω cm when growth temperatures were above 620 °C.

One of the most interesting investigations was the growth of $In_xGa_{1-x}N$ at low temperatures (60, 200 and 400 °C) carried out by Beierlein et al. [95] on glass substrate by a plasma-enhanced MBE process. As expected, all samples were found to be n-type. Those samples grown at 400 °C showed a strong increase in the carrier concentration with increasing InN composition across the entire alloy range, whereas for the unheated substrate series, the carrier concentration appeared to be insensitive to the mole fraction for InN-rich alloys. Apart from that, the resistivity of the samples was found to be weakly dependent on the growth temperature; however, it decreased rapidly with increasing InN mole fraction. The mobility of $In_xGa_{1-x}N$ showed marked improvement as the growth temperature was increased. The mobility was also observed to be relatively insensitive to the change of InN mole fraction for $x > 0.6$. However, for $x < 0.5$, the mobility fell steeply with decreasing InN content. Similar low-temperature (500 °C) growth of InGaN films on glass substrates using rf plasma excitation was also investigated by Sato et al. [96]. In their work, InGaN films with InN content up to 50% were grown. Their results showed that the resistivity of the samples decreased with increasing In content. On the other hand, both mobility and carrier density were found to be increased with increasing In content.

4. Vegard's law and bowing

Precise knowledge of the band gap as a function of alloy composition is essential for the design and fabrication of new optoelectronic device structures. Vegard's law is commonly used to estimate the composition of ternary materials from extrapolating from the endpoint binaries. The energy gap of $In_xGa_{1-x}N$ is given by the composition-weighted average of the GaN and InN gaps, and can be approximated by

$$E_g(x) = xE_g(\mathrm{InN}) + (1-x)\mathrm{E}_g(\mathrm{GaN}) \tag{1}$$

where the band gaps of wurtzite GaN and InN at 300 K are $E_g(\mathrm{GaN}) = 3.39$ eV [97], $E_g(\mathrm{InN}) = 0.7$ eV [1], respectively.

Accuracy can be improved using this standard equation, in which a third term with a "bowing" parameter, b, is added.

$$E_g(x) = xE_g(\mathrm{InN}) + (1-x)E_g(\mathrm{GaN}) - bx(1-x). \tag{2}$$

By taking into account the non-linear effects of alloying, the bowing parameter, b, in fact, measures the deviation from a linear interpolation between InN and GaN. Both experimental and theoretical studies have been carried out extensively to determine the value of the bowing parameter. However, the bowing parameter has not been concluded yet. The presence of strain, phase separation and inhomogeneities in InGaN as well as the techniques used to measure the indium composition and band gap energy of InGaN could lead to the inaccuracy of determining the bowing parameter.

Bowing parameter values ranging from 1 to 6 eV have been reported. The large scatter of the published values suggests that it is difficult to get universal agreement on the bowing parameter, since InGaN samples were grown by different techniques and different conditions. However, the large value and strong composition dependence of the bowing parameter are not surprising, in view of the large lattice mismatch of these two binaries. Table 1 shows some of the reported values given in the literature.

4.1. Factors contributing to the inaccuracy of bowing parameter

Current modern optoelectronic devices contain very thin (2–3 nm) quantum wells of InGaN in which the light emission characteristics are determined by the combination of the indium composition and the layer thickness. These two factors determine the band gap and strain of the InGaN. The strain between the well and barrier will induce a piezoelectric field which leads to the anomalous behaviour of the quantum-confined Stark effect.

For precise determination of the composition-dependent InGaN band gap, the band gap should be measured by photoreflection [113] or spectroscopic ellipsometry [114] rather than from PL. This is because the InGaN near band edge PL spectrum is Stokes shifted relative to the band edge, leading to an underestimate of the energy gap [115]. Wetzel [102] and McCluskey [103] reported a much smaller bowing parameter using photoreflection (PR) spectroscopy and optical transmission (OT) measurements as compared to PL. However, they pointed out that the difference in bowing parameter estimation resulted from the indium composition determination by XRD measurement. The thin InGaN layer grown on GaN was greatly strained by biaxial compressive stress which caused a blue-shift of the band gap as compared to the unstrained InGaN. Therefore, the band gap of unstrained InGaN is expected to be smaller than that determined by a similar technique [107]. Since the sources of erroneous measurements have led to the inaccuracy of the alloy composition, at present no common agreement is established for the use of Vegard's law in determination of the indium content. Furthermore, first-principles calculations found that the bowing parameter should vary significantly with composition [101], and the claim was confirmed by the work done by Shen et al. [99].

High-resolution XRD (HR-XRD) is almost exclusively used for determination of lattice parameters of the semiconductor thin films, in which the chemical composition is deduced by applying Vegard's law. However, this unique relationship between lattice parameters and chemical composition is valid only for the relaxed lattice parameters [116,117]. Typically, XRD is used to measure the lattice constant along the c axis. The InN concentration is then determined by linear interpolation between the lattice constant of InN and GaN (Vegard's law). When the InGaN layers experience biaxial compression, the unit cell will be distorted, and the lattice constant along c axis is elongated, resulting in a systematic overestimation of the InN composition [101,103], and this corresponds to underestimate of the bowing parameter. Therefore, the composition of InGaN alloy should be assessed not only by XRD, but also by chemical analysis to serve as an independent reference. The presence of strain effects will complicate the determination of the composition by XRD which requires the use of the correct elastic parameters of the InGaN [98]. Chemical techniques such as Rutherford backscattering spectroscopy (RBS), secondary ion mass spectroscopy (SIMS) and electron probe microanalysis (EPMA) can be used alternatively to analyze the chemical composition, and they are insensitive to the strain state of the samples; however, relatively thick samples are required [118]. The use of HR-XRD combined with RBS to determine the chemical composition of InGaN/GaN MQWs had been reported by Zhou et al. [119].

The band gap of InN has been recently discovered to be smaller than 1.0 eV [1–7], rather than the previously accepted value of 1.9 eV [131]. Early studies on sputtered InN films with high electron concentration revealed a large Burstein–Moss shift in the optical absorption edge which could be responsible for the 1.9 eV band gap reported previously for some degenerately doped InN films [132]. Although the revised InN band gap is generally recognized as about 0.7 eV, the controversy about the correct band gap energy is still an ongoing subject. The "classical" 1.9 eV InN band gap value was still strongly supported by several groups [8–10,133], in which

Table 1
The bowing parameter, b, reported by different groups

Composition measurement	Thickness (nm)	Indium content (x)	E_g measurement	Bowing parameter, b (eV)	Strain state	Growth technique	Reference
XRD	300	0.2–0.27	PL	3.6	Strained	MBE	[58]
SIMS	15–60	0.02–0.15	PR	3.2	Strained	MOCVD	[98]
XRD	400	$x < 0.10$ $x > 0.13$	PL	6.0 4.0	Relaxed	MBE	[99]
XRD	N.A.	0.07–0.33	PL	1.0	N.A.	MOCVD	[100]
N.A.	N.A.	$x = (0.0625,$ 0.125, 0.25)	F.P.C.	$b = (4.8,$ 3.5, 3.0)	Relaxed	N.A.	[101]
			PR	2.6	Strained		
XRD	40	$0 < x < 0.2$	PR	3.8	Relaxed	MOCVD	[102]
			PL	3.2	Strained		
RBS	250	$x \leq 0.12$	OT	3.5	Strained	MOCVD	[103]
F.P.C.	F.P.C.	F.P.C.	F.P.C.	1.7	N.A.	N.A.	[104]
Simulation	N.A.	0–0.375	Simulation	1.21 ± 0.03	Relaxed	N.A.	[105]
XRD	250	$0.61 < x < 1.0$	PL	1.8	Relaxed	MBE	[106]
XRD	40	0–0.2	PL	3.2	Strained	MOCVD	[107]
XRD	30–100	0–0.25	PL	4.11 3.42	Relaxed Strained	MOCVD	[108]
N.A.	200–7500	0–0.5	OA	1.4	N.A.	MBE	[109,110]
F.P.C.	F.P.C.	F.P.C.	F.P.C.	1.782–1.916	N.A.	N.A.	[111]
N.A.	N.A.	N.A.	Modeling	2.72	N.A.	N.A.	[112]

Note: F.P.C.: First-principles calculation; SIMS: Secondary ion mass spectroscopy; RBS: Rutherford backscattering spectroscopy; OA: Optical absorption; N.A.: Information not available, or not applicable.

experimental data have been presented to substantiate their claim. Table 2 summarizes some of the InN band gap found from the literature in or after year 2002: a relatively large statistical distribution of the reported InN band gap can be observed in Table 2. The failure in obtaining a common agreed InN band gap energy would lead to the inaccuracy in computing the optical properties of the InN-based ternary and quaternary materials.

Obviously, the bowing parameter is found to be influenced by the optical technique used to determine the band gap, the quality of the materials (for instance, strain, phase separation and inhomogeneity), and the measurement of the exact indium content of the alloy, as well as the precise knowledge of the energy band gap of the constituent binary materials.

5. Determination of indium composition by XRD

At present, most of the InGaN alloys with different indium composition have been widely used as quantum wells which serve as the active region of the optoelectronic devices. Since the InGaN epilayer used for this purpose is very thin, it is very difficult to determine the indium content accurately.

The indium composition of InGaN has been commonly assessed by XRD measurements. Indium compositions derived from XRD measurements depend on an interpretation of averaged lattice constants, which proves to be extremely difficult in the presence of phase-segregated indium-rich quantum dots [134]. Furthermore, XRD is a direct technique used to measure

Table 2
Some of the InN band gap energies reported in the literature

Growth method	Growth temp. (°C)	Thickness (nm)	E_g measurement	E_g (eV)	Reference
MBE	–	120–1000	OA, PL, PR	0.7–0.8	[1]
RPE-CVD	200–550	–	OA	0.9–2.3	[120]
MBE	∼520	2.3–5.7	PL	∼0.7	[36]
MBE	550	250	PL	0.66	[106]
MBE	580–630	800–5500	OR, OT	0.59–0.65	[121]
Sputtering	100	2200	PL, OA	1.87, 1.97	[8]
MBE	–	800–1000	VEELS	1.7±0.2	[9]
Sputtering	<30	–	OA	2.14–2.3	[10]
HP-CVD	527–727	–	OA	0.83–1.34	[122]
–	–	–	TS	2.06	[123]
–	–	–	TS	0.85±0.1	[124]
MOCVD	–	–	PL	0.83	[125]
RPE-CVD	300–500	Thin to thick	OA	1.1–1.8	[126]
MOVPE	550	500	Reflectivity, PL	1.2, 0.77	[127]
MBE	450-600	–	PL	0.62–0.65	[128]
MOCVD	500	–	PL, OT	∼1.2	[129]
MBE	200–500	–	OA, PL	1.1–1.8	[130]

Note: HP-CVD: High-pressure CVD; OR: Optical reflectance; OT: Optical transmission; PR: Photoreflection; RPE-CVD: Remote plasma-enhanced CVD; TS: Theoretical study; VEELS: Valence electron energy-loss spectroscopy.

the structural parameters and it determines the indium composition indirectly. Therefore, with the presence of lattice strain, this technique may result in erroneous measurements of the composition.

The lattice mismatch between GaN and InN is about 10%; therefore the growth of InGaN on GaN will lead to strain in the InGaN layer. When the thickness of the InGaN epilayer is smaller than the critical thickness, the InGaN will be pseudomorphically strained, in which the in-plane lattice constant of the InGaN epilayer matches to the GaN substrate. However, when the critical thickness is exceeded, strain relaxation occurs through the introduction of extended defects [101]. Akasaki et al. [135] studied the critical thickness of InGaN on GaN with indium molar fraction below 20%; they reported that the critical thicknesses were much larger than those calculated from the Mathews and Blakeslee (M–B) model [136] and the Fischer model [137]. The experimental values of the critical thickness were observed to be independent of the InN molar fraction. Fig. 5 shows that critical thickness of the InGaN on GaN as compared to the M–B and Fischer models.

For a hexagonal unit cell, the interplanar spacing, d, of the $(hkil)$ plane is given by

$$\frac{1}{d_{hkl}^2} = \frac{4}{3}\frac{h^2 + k^2 + hk}{a^2} + \frac{l^2}{c^2} \tag{3}$$

where a and c are the lattice parameters. Symmetric XRD reflections from $(000l)$ in the growth direction of InGaN allow the measurement of lattice constant, c, which is easier to be obtained experimentally [138]. Moreover, from Bragg's law, the lattice constant, c, for any allowed $(000l)$ reflection can be derived as

$$c = l\lambda/(2\sin\theta). \tag{4}$$

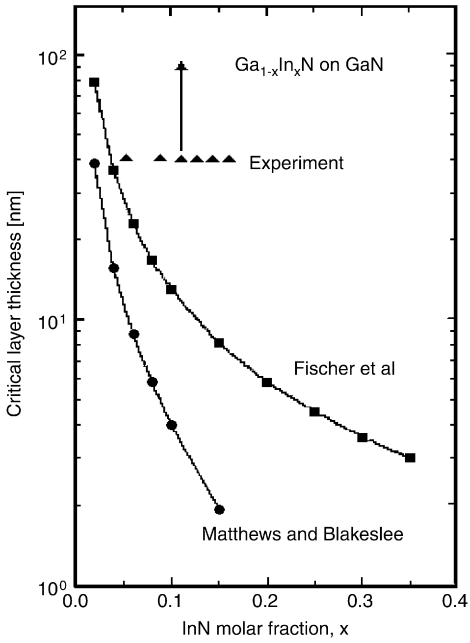

Fig. 5. Critical thickness (t_c) of $In_xGa_{1-x}N$ grown on GaN. Solid circle and square show the t_c estimated from the Mathews and Blakeslee model, and the Fisher model, respectively. (After Ref. [135]. Reproduced from I. Akasaki, H. Amano, 36 (1997) 5393 with permission from Japan J. Appl. Phys.).

This lattice constant can be used to determine the indium composition by the application of Vegard's law. To determine the indium composition from XRD measurements, usually two different assumptions are considered for the state of strain [118,139,140].

In the first assumption, the InGaN epilayer is larger than the critical thickness; the layer may be fully relaxed. This assumption is likely to be justified when the layers are relatively thick. In the absence of strain in the InGaN epilayer, the actual lattice constant of the relaxed InGaN epilayer corresponds to the measured value, $c_{\mathrm{InGaN}} = c_o$. The variation of indium composition is usually assumed to be linear, as in Vegard's law:

$$c_{\mathrm{InGaN}} = x c_{\mathrm{InN}} + (1 - x) c_{\mathrm{GaN}} \tag{5}$$

from which x can be determined by

$$x = \frac{(c_o - c_{\mathrm{GaN}})}{(c_{\mathrm{InN}} - c_{\mathrm{GaN}})}. \tag{6}$$

However, the inaccuracy of x may arise from errors in the lattice parameters for GaN and InN, since the value of lattice parameters are found to be different in the literature [141].

In the second assumption, the InGaN epilayer is smaller than the critical thickness; the layer may be pseudomorphic. In pseudomorphic growth, a thin epilayer accommodates itself to a thick substrate; in this case, it is assumed that $a_{\mathrm{InGaN}} = a_{\mathrm{GaN}}$. This is usually the case for a thin InGaN epilayer with thickness less than 75 nm [118]. Wagner et al. [98] studied the band gap energy of strained hexagonal InGaN layers on GaN with $x \leq 0.15$. InGaN layers with typical thickness of 30 nm are found to be pseudomorphically strained to the in-plain lattice parameter of the GaN layer as confirmed by HR-XRD measurements. Fig. 6 shows the plot of c versus a

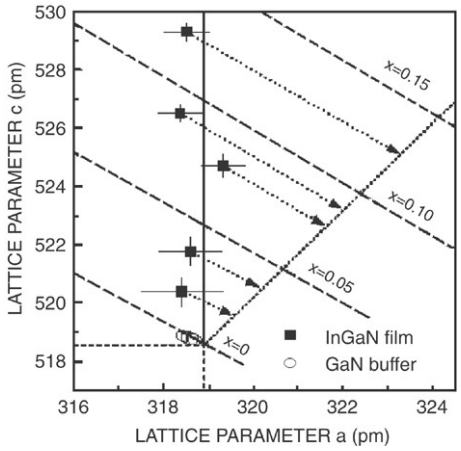

Fig. 6. c versus a lattice parameters as determined by HR-XRD for a 30 nm thick InGaN layer grown on GaN. (After Ref. [98]. Reproduced from J. Wagner, A. Ramakrishnan, D. Behr, M. Maier, N. Herres, M. Kunzer, H. Obloh, K.-H. Bachem, Internet J. Nitride Semicond. Res. 4S1 (1999) G2.8, with permission from MRS).

lattice parameters for InGaN layers with a thickness of 30 nm. For biaxially strained wurtzite structures, InGaN/GaN, the unit cell is distorted. In order to separate the influence of strain and composition effects on c_{InGaN}, both lattice parameters, a_{InGaN} and c_{InGaN}, have to be measured. Therefore, from Hooke's law, x can be determined by solving [139,140]

$$[c_{\mathrm{InGaN}} - c_o(x)] + 2\frac{C_{13}(x)c_o(x)}{C_{33}(x)a_o(x)}[a_{\mathrm{InGaN}} - a_o(x)] = 0 \tag{7}$$

where symbols with subscript of o and InGaN are the relaxed and measured lattice parameters respectively, $C_{ij}(x)$ are the linearly interpolated elastic constants from the binary semiconductors. By measuring c_{InGaN}, and solving Eq. (7), x can be determined. However, a wide variation of the published values for these elastic constants of GaN has led to the inaccuracy of the determination of indium composition [142]. As pointed out by Yamaguchi et al. [143], the measured elastic constants of thin GaN epitaxial films could be significantly different from actual values, due to the presence of residual strains.

On the other hand, the indium composition also can be derived indirectly from the reciprocal space map (RSM). The studies revealed that the strain can be determined directly by measuring the RSM for an asymmetric reflection [138,144–147] or alternatively by scanning on both a symmetric and an asymmetric reflection [117,138]. Once the strain state of the thin film is analyzed, the indium composition of InGaN alloy can be determined from the RSM [146,148].

Apart from that, the effect of lattice strain can be taken into account or overcome by employing both symmetric and asymmetric XRD scans, in order to measure the lattice constants c and a, respectively [116]. Both c and a can be calculated from Eq. (3). The indium content can be determined using the relation [149]

$$x = -\frac{ac(1+\nu) - ac_o^{\mathrm{GaN}} - a_o^{\mathrm{GaN}}c\nu}{ac_o^{\mathrm{GaN}} - ac_o^{\mathrm{InN}} - a_o^{\mathrm{InN}}c\nu + a_o^{\mathrm{GaN}}c\nu} \tag{8}$$

where $\nu = -\varepsilon_c/\varepsilon_a$, ε_c and ε_a are the strains along the c and a axes, respectively. In a planar biaxially strained wurtzite crystal, it also can be simplified to $\nu = 2C_{13}/C_{33}$. Similarly, the

inaccuracy of x arises from the uncertainties of these elastic constants. In addition, the error of calculating indium composition also may come from the poor accuracy in the measurement of a. Better accuracy can be achieved by using higher a-index planes [116].

6. Indium segregation and piezoelectricity

Recently, there has been much debate on the emission mechanism in the InGaN alloys. From the literature, two different radiative recombination mechanisms for this unique alloy have been reported. The large Stokes shift between absorption and emission is the first mechanism claimed by many groups [115,150–155]; it is attributed to the effect of exciton localization caused by spatial indium fluctuations or phase separation in InGaN: possibly, the self-organized QDs. In contrast, other groups [107,156–158] presented the second radiative recombination mechanism which was claimed to be due to the quantum-confined Stark effect (QCSE) induced by large internal electric fields. However, Kawakami et al. [159] pointed out that the discrepancy could be attributed to the insufficient information provided by optical data, and the degree of localization, as well as the contribution from internal electric fields, is different from sample to sample, due to the differences in the growth techniques and growth conditions.

In the first model, the phase separation that leads to the inhomogeneity of the indium concentration is due to the large miscibility gap which has been predicted from the InGaN phase diagram. At typical growth temperatures of 700–800 °C, InGaN is known to be thermodynamically unstable for the incorporation of even moderate indium concentration [23]. The formation of InN nanoclusters or quantum dots resulting from the phase segregation in InGaN has been evidenced in the works carried out by few groups [152,161–164], where optical and structural studies on the MOCVD-grown samples revealed the presence of spatial indium fluctuations. The exciton localization in the QDs was considered to be the reason leading to the unique light emission characteristics of the InGaN alloy. The exciton localization shows many promising effects on the performance of the InGaN-based optoelectronic devices; for instance, it determines the emission energy in LEDs and contributes to optical gain in laser structures [160]. On the other hand, if the indium composition is randomly distributed, and if the well barrier interface is atomically flat, the effect of localization will be very small [159].

In the second model, the quantum-confined Stark effect (QCSE) recombination mechanism is ascribed to the presence of a large piezoelectric field in the well. This piezoelectric field is caused by strain which originates from the lattice mismatch between GaN and InGaN. It has also been claimed that the presence of huge electrical fields in III-nitrides QWs is due to their wurtzitic symmetry [165–167]. This internal electrical field separates the carriers along the growth axis, leading to a strong reduction of the oscillator strength for wide QWs. Consequently, the radiative lifetime drastically increases, making it easier for the carriers to recombine non-radiatively at dislocations [42]. The existence of an internal electric field has been reported in InGaN QWs, in which the PL red-shift was observed as compared to those InGaN films with relatively high thickness but having same chemical composition as that of the QW layer [42,107,168].

The study from Shapiro et al. [169] showed that both indium phase separation and piezoelectric field effects are involved in the radiative recombination processes. Their investigation revealed that indium phase separation effects are dominant in the structures where the average indium amount is high, whereas piezoelectric effects are likely to dominate in relatively thick wells ($L > 3$ nm) with low indium content ($x < 0.15$). In addition, Ochalski et al. [170] investigated and compared PL and PR spectra on a series of InGaN/GaN QWs grown under identical conditions except for the growth time of the InGaN layers. Their results

showed that samples which emit from the blue to red can provide only partial conclusion if both localization effect and QCSE are not taken into consideration. Similarly, Grandjean et al. [42] also reported that, based on their experimental works carried out on GaN/AlN QDs and InGaN/GaN QWs, both the localization effect and QCSE are observed to be responsible for the optical recombination. An in-depth study of these two different radiative recombination mechanisms was also carried out by Monemar et al. [171,172]. In their work, $In_{0.15}Ga_{0.85}N$/GaN MQW samples with different growth temperature and donor doping concentration have been prepared and used in their investigation. From the study, they found that the piezoelectric field played an important role in the recombination process. They argued that the recombination was mainly caused by separately localized electron and holes in the QW potential which was severely distorted by the piezoelectric field. Strong potential fluctuations were also present which determined the width of the PL peak. These fluctuations were enhanced by the piezoelectric field, but weakened by the lateral electron screening effect. On the other hand, it has been shown that the presence of phase separation was minimal when InGaN layers were grown by MOCVD at 750 °C; however, for growth above this temperature, phase separation would occur and separate domains were created in the layer [173,174]. Therefore, Monemar et al. [171] concluded that by lowering the InGaN growth temperature to 700 °C, the short-range potential fluctuations which were related to indium segregation could be removed.

Apart from this, in the radiative recombination process, Stokes-like shift or blue-shift of emission energy with increasing photo-excitation intensity cannot be ascribed solely to the effect of exciton localization as pointed out by Kawakami et al. [159]. This is due to large internal electric fields that modify the absorption edge of InGaN quantum wells by the quantum-confined Franz–Keldysh effect (QCFK) and QCSE [175]. Furthermore, the presence of certain phenomena in macroscopic optical spectroscopy that cannot be interpreted by QCFK and/or QCSE effects: for example, the anomalous temperature dependence of emission peak energies, the "almost temperature independence" of radiative recombination lifetimes and the mobility edge behaviour.

7. Conclusions

In summary, we have reviewed the fundamental properties of $In_xGa_{1-x}N$. The growth parameters such as growth temperatures, V/III ratios, and growth rates as well as growth pressure which link closely to the quality of the InGaN epilayers are briefly described. An insight into the basic properties of the InGaN alloys such as optical, structural and electrical characteristics is also presented. In addition, Vegard's law and the bowing parameter, as well as major factors contributing to uncertainties of the bowing parameter of InGaN, are compiled and discussed. Apart from that, the determination of indium composition by XRD using different assumptions and various equations are summarized. Finally, different emission mechanisms of the strained InGaN quantum wells are also discussed. The potential of InGaN for fabrication of novel and high performance optoelectronic devices is immense; however, a great deal of experimental and theoretical works are still needed, so that the fundamental properties of this material can be further explored and developed.

Search strategy and selection criteria

The articles were searched and compiled in this topical review article by using the key word "InGaN" alone, or together with other keywords such as "bowing parameter", "PL", "XRD" and "InN". Many articles were selected from the past five years in which the new band gap of InN

was discovered and reported to be 0.7 eV in the year 2002. However, many old articles were also quoted. It is undeniable that some of the relatively old articles remained influential; they are still having significant impact on building up the technological framework and contributing immense scientific interest in InGaN technology.

Acknowledgements

Support from IRPA RMK-8 Strategic Research grant and Universiti Sains Malaysia is gratefully acknowledged.

References

[1] J. Wu, W. Walukiewicz, K.M. Yu, J.W. Ager III, E.E. Haller, H. Lu, W.J. Schaff, Y. Saito, Y. Nanishi, Appl. Phys. Lett. 80 (2002) 3967.
[2] Y. Saito, H. Harima, E. Kurimoto, T. Yamaguchi, N. Teraguchi, A. Suzuki, T. Araki, Y. Nanishi, Phys. Status Solidi b 234 (2002) 796.
[3] V.Yu. Davydov, A.A. Klochikhin, R.P. Seisyan, V.V. Emtsev, S.V. Ivanov, F. Bechstedt, J. Furthmuller, H. Harima, A.V. Mudryi, J. Aderhold, O. Semchinova, J. Graul, Phys. Status Solidi b 229 (2002) R1.
[4] T. Matsuoka, H. Okamoto, M. Nakao, H. Harima, E. Kurimoto, Appl. Phys. Lett. 81 (2002) 1246.
[5] B. Monemar, P.P. Paskov, A. Kasic, Superlatt. Microstruct. 38 (2005) 38.
[6] B. Arnaudov, T. Pashkova, P.P. Paskov, B. Magnusson, E. Valcheva, B. Monemar, H. Lu, W.J. Schaff, H. Amano, I. Akasaki, Phys. Rev. B 69 (2004) 115216.
[7] W. Walukiewicz, S.X. Li, J. Wu, K.M. Yu, J.W. Ager III, E.E. Haller, H. Lu, W.J. Schaff, J. Cryst. Growth 269 (2004) 119.
[8] Q.X. Guo, T. Tanaka, M. Nishio, H. Ogawa, X.D. Pu, W.Z. Shen, Appl. Phys. Lett. 86 (2005) 231913.
[9] P. Specht, J.C. Ho, X. Xu, R. Armitage, E.R. Weber, R. Erni, C. Kisielowski, Solid State Commun. 135 (2005) 340.
[10] K.S.A. Butcher, M. Winttrebert-Fouquet, P.P.-T. Chen, T.L. Tansley, H. Dou, S.K. Shrestha, H. Timmers, M. Kuball, K.E. Prince, K.E. Bradby, J. Appl. Phys. 95 (2004) 6124.
[11] S.J. Pearton, J.C. Zolper, R.J. Shul, F. Ren, J. Appl. Phys. 86 (1999) 1.
[12] S.J. Pearton, F. Ren, A.P. Zhang, K.P. Lee, Mater. Sci. Eng. R 30 (2000) 55.
[13] S.N. Mohammad, H. Morkoc, Prog. Quantum Electron. 20 (1996) 361.
[14] S.P. Denbaar, Proc. IEEE 85 (1997) 1740.
[15] R.F. Davis, A.M. Roskowski, E.A. Preble, J.S. Speck, B. Heying, J.A. Feitas, E.R. Glaser Jr., W.E. Carlos, Proc. IEEE 90 (2002) 993.
[16] M.A. Reshchikov, H. Morkoc, J. Appl. Phys. 97 (2005) 061301.
[17] O. Ambacher, J. Phys. D: Appl. Phys. 31 (1998) 2653.
[18] H. Morkoc, S. Strite, B.G. Gao, M.E. Lin, B. Sverdlov, M. Burns, J. Appl. Phys. 76 (1994) 1363.
[19] A.G. Bhuiyan, A. Hashimoto, A. Yamamoto, J. Appl. Phys. 94 (2003) 2779.
[20] T. Matsuoka, Superlatt. Microstruct. 37 (2005) 19.
[21] Y. Nanishi, Y. Saito, T. Yamaguchi, Japan J. Appl. Phys. 42 (2003) 2549.
[22] G. Popovici, H. Morkoc, in: S.J. Pearton (Ed.), GaN and Related Materials II, Gordon and Breach Science, Netherlands, 2000, p. 93.
[23] I. Ho, G.B. Stringfellow, Appl. Phys. Lett. 69 (1996) 2701.
[24] T. Nagatomo, T. Kuboyama, H. Minamino, O. Omoto, Japan J. Appl. Phys. 28 (1989) L1334.
[25] N. Yoshimoto, T. Matsuoka, T. Sasaki, A. Katsu, Appl. Phys. Lett. 59 (1991) 2251.
[26] E.L. Piner, F.G. McIntosh, J.C. Roberts, M.E. Aumer, V.A. Joshkin, S.M. Bedair, N.A. El-Masry, MRS Internet J. Nitride Semicond. Res. 1 (1996) 43.
[27] W. Van der Stricht, I. Moerman, P. Demeester, L. Considine, E.J. Thrush, J.A. Crawley, MRS Internet J. Nitride Semicond. Res. 2 (1997) 16.
[28] P. Waltereit, O. Brandt, K.H. Ploog, M.A. Tagliente, L. Tapfer, Phys. Status Solidi b 228 (2001) 49.
[29] R.A. Oliver, M.J. Kappers, C.J. Humphrey, G.A.D. Briggs, J. Cryst. Growth 273 (2004) 393.
[30] S. Keller, B.P. Keller, D. Kapolnek, A.C. Abare, H. Masui, L.A. Coldren, U.K. Mishra, S.P. Den Baars, Appl. Phys. Lett. 68 (1996) 3147.

[31] S. Keller, B.P. Keller, D. Kapolnek, S.P. Den Baars, I.K. Shmagin, R.M. Kolbas, S. Krishnankutty, J. Cryst. Growth 170 (1997) 349.
[32] T. Matsuoka, N. Yoshimoto, T. Sasaki, A. Katsui, J. Electron. Mater. 21 (1992) 157.
[33] S. Keller, S.F. Chichibu, M.S. Minsky, E. Hu, U.K. Mishra, S.P. Den Baars, J. Cryst. Growth 195 (1998) 285.
[34] S.-N. Lee, S. Tan, W. Lee, H. Paek, M. Seon, I.-H. Lee, O. Nam, Y. Park, J. Cryst. Growth 250 (2003) 256.
[35] D.-J. Kim, Y.-T. Moon, I.-H. Lee, S.-J. Park, J. Electron. Mater. 30 (2001) 99.
[36] H. Naoi, M. Kurouchi, D. Muto, T. Araki, T. Miyajima, Y. Nanishi, J. Cryst. Growth 288 (2006) 283.
[37] P. Laukkanen, S. Lehkonen, P. Uusimaa, M. Pessa, A. Sepala, T. Ahlgren, E. Rauhala, J. Cryst. Growth 230 (2001) 503.
[38] M.A. Herman, H. Sitter, Molecular Beam Epitaxy, in: M.B. Panish (Ed.), Springer Series in Materials Science, Springer, New York, 1989.
[39] H. Chen, R.M. Feenstra, J. Northrup, D.W. Greve, MRS Internet J. Nitride Semicond. Res. 6 (2001) 11.
[40] K. Kushi, H. Sasamoto, D. Sugihara, S. Nakamura, A. Kikuchi, K. Kishino, Mater. Sci. Eng. B 59 (1999) 65.
[41] T. Bottcher, S. Einfeldt, V. Kirchner, S. Figge, H. Heinke, D. Hommel, H. Selke, P.L. Ryder, Appl. Phys. Lett. 73 (1998) 3232.
[42] N. Grandjean, B. Damilano, J. Massies, J. Phys.: Condens. Matter 13 (2001) 6945.
[43] H.-C. Lin, C.-K. Shu, J. Ou, Y.-C. Pan, W.-K. Chen, W.-H. Chen, M.-C. Lee, J. Cryst. Growth 189–190 (1998) 57.
[44] W. Van der Stricht, I. Moerman, P. Demeester, J.A. Crawley, E.J. Thrush, J. Cryst. Growth 170 (1997) 344.
[45] Y.Z. Tong, F. Li, G.Y. Zhang, Z.J. Yang, S.X. Jin, X.M. Ding, Z.Z. Gan, Solid State Commun. 109 (1999) 173.
[46] C.R. Lee, S.J. Son, I.-H. Lee, J.Y. Leem, S.K. Noh, J. Cryst. Growth 182 (1997) 6.
[47] S.M. Bedair, F.G. McIntosh, J.C. Roberts, E.L. Piner, K.S. Boutros, N.A. El-Mastry, J. Cryst. Growth 178 (1997) 32.
[48] N. Grandjean, J. Massies, Mater. Sci. Eng. B 59 (1999) 39.
[49] A. Sohmer, J. Off, H. Bolay, V. Harle, V. Syganow, J.S. Im, V. Wagner, F. Adler, A. Hangleiter, A. Dornen, F. Scholz, D. Brunner, O. Ambacher, H. Lakner, MRS Internet J. Nitride Semicond. Res. 2 (1997) 14.
[50] S. Nakamura, M. Senoh, N. Iwasa, S. Nagahama, Japan J. Appl. Phys. 34 (1995) L797.
[51] Y.-L. Lai, C.-P. Liu, Z.-Q. Chen, Thin Solid Films 498 (2006) 128.
[52] R.W. Martin, P.R. Edwards, R. Pecharroman-Galego, C. Liu, C.J. Deatcher, I.M. Watson, K.P. O'Donnell, J. Phys. D: Appl. Phys. 35 (2002) 604.
[53] J.C. Harris, H. Brisset, T. Someya, Y. Arakawa, Japan J. Appl. Phys. 38 (1999) 2613.
[54] H.Y. Cho, J.Y. Lee, C.S. Kim, G.M. Yang, J. Electron. Mater. 30 (2001) 1348.
[55] B. Damilano, N. Grandjean, C. Pernot, J. Massies, Japan J. Appl. Phys. 40 (2001) L918. Pt.2, 9A/B.
[56] P. Lefebvre, T. Taliercio, S. Kalliakos, A. Morel, X.B. Zhang, M. Gallart, T. Bretagnon, B. Gil, N. Grandjean, B. Damilano, J. Massies, Phys. Status Solidi b 228 (2001) 65.
[57] S.F. Chichibu, A.C. Abare, M.P. Mack, M.S. Minsky, T. Deguchi, D. Cohen, P. Kozodoy, S.B. Fleischer, S. Keller, J.S. Speck, J.E. Bowers, E. Hu, U.K. Mishra, L.A. Coldren, S.P. DenBaars, K. Wada, T. Sota, S. Nakamura, Mater. Sci. Eng. B 59 (1999) 298.
[58] F.B. Naranjo, S. Fernandez, M.A. Sanchez-Garcia, F. Calle, E. Calleja, A. Trampert, K.H. Ploog, Mater. Sci. Eng. B 93 (2002) 131.
[59] D.-J. Kim, Y.-T. Moon, K.-M. Song, C.-J. Choi, Y.-W. Ok, T.-Y. Seong, S.-J. Park, J. Cryst. Growth 221 (2000) 368.
[60] M.G. Cheong, E.-K. Suh, H.J. Lee, Semicond. Sci. Technol. 16 (2001) 783.
[61] N. Grandjean, J. Massies, S. Dalmasso, P. Vennegnes, L. Siozande, L. Hirsch, Appl. Phys. Lett. 74 (1999) 3616.
[62] K. Uchida, M. Kawata, T. Yang, S. Toto, T. Mishima, A. Niwa, J. Gotoh, J. Electron. Mater. 28 (1999) 246.
[63] P. Hurst, P. Dawson, S.A. Levetas, M.J. Godfrey, I.M. Watson, G. Duggan, Phys. Status Solidi b 228 (2001) 137.
[64] T.-C. Wen, W.-I. Lee, Japan J. Appl. Phys. 40 (2001) 5302.
[65] S. Kim, K. Lee, K. Park, C.-S. Kim, J. Cryst. Growth 247 (2003) 62.
[66] D.-J. Kim, Y.-T. Moon, K.-M. Song, S.-J. Park, Japan J. Appl. Phys. 40 (2001) 3085.
[67] S. Nakamura, Mater. Sci. Eng. B 43 (1997) 258.
[68] S. Nakamura, Microelectron. J. 25 (1994) 651.
[69] S. Keller, U.K. Mishra, S.P. DenBaars, W. Seifert, Japan J. Appl. Phys. 37 (1998) L431.
[70] W.K. Burton, N. Cabrera, F.C. Frank, Trans. R. Soc. Ser. A 243 (1951) 300.
[71] S.K. Shee, Y.H. Kwon, J.B. Lam, G.H. Gainer, G.H. Park, S.J. Hwang, B.D. Little, J.J. Song, J. Cryst. Growth 221 (2000) 373.
[72] K. Uchida, M. Kawata, T. Yang, A. Miwa, J. Gotoh, Japan J. Appl. Phys. 37 (1998) L571.
[73] K. Uchida, M. Kawata, T. Yang, S. Goto, T. Mishima, A. Miwa, J. Gotoh, J. Electron. Mater. 28 (1999) 246.

[74] S.-J. Leem, M.H. Kim, J. Shin, Y. Choi, J. Jeong, Japan J. Appl. Phys. 40 (2001) L371.
[75] L.W. Ji, Y.K. Su, S.J. Chang, L.W. Wu, T.H. Fang, J.F. Chen, T.Y. Tsai, Q.K. Xue, S.C. Chen, J. Cryst. Growth 249 (2003) 144.
[76] L.W. Ji, Y.K. Su, S.J. Chang, S.H. Liu, C.K. Wang, S.T. Tsai, T.H. Fang, L.W. Wu, Q.K. Xue, Solid State Electron. 47 (2003) 1753.
[77] M.G. Cheong, E.-K. Suh, H.J. Lee, J. Lumin. 99 (2002) 265.
[78] M. Kauer, S.E. Hooper, V. Bousquet, K. Johnson, C. Zellweger, J.M. Barnes, J. Windle, T.M. Smeeton, J. Heffernan, Sharp Tech. J. 92 (2005) 72.
[79] M. Kauer, J. Heffernan, S.E. Hooper, V. Bousquet, K. Johnson, C. Zellweger, Proc. SPIE 5738 (2005) 245.
[80] S.E. Hooper, M. Kauer, V. Bousquet, K. Johnson, C. Zellweger, J. Heffernan, J. Cryst. Growth 278 (2005) 361.
[81] J. Heffernan, M. Kauer, S.E. Hooper, V. Bousquet, K. Johnson, Phys. Stat. Solidi a 12 (2004) 2688.
[82] X.-Q. Shen, T. Ide, M. Shimizu, H. Hara, H. Okumura, Japan J. Appl. Phys. 39 (2000) L1270.
[83] X.-Q. Shen, T. Ide, M. Shimizu, F. Sasaki, H. Okumura, Phys. Status Solidi b 228 (2001) 99.
[84] X.-Q. Shen, T. Ide, S.H. Cho, M. Shimizu, H. Hara, H. Okumura, S. Sonoda, S. Shimizu, Japan J. Appl. Phys. 39 (2000) L16.
[85] X.-Q. Shen, T. Ide, S.H. Cho, M. Shimizu, H. Hara, H. Okumura, S. Sonoda, S. Shimizu, J. Cryst. Growth 218 (2000) 115.
[86] E.S. Hellman, MRS Internet J. Nitride Semicond. Res. 3 (1998) 11.
[87] M. Stutzmann, O. Ambacher, M. Eickhoff, U. Karrer, A. Lima Pimenta, R. Neuberger, J. Schalwig, R. Dimitrov, P.J. Schuck, R.D. Grober, Phys. Status Solidi b 228 (2001) 505.
[88] P. Prystawko, M. Leszczynski, A. Sliwinski, H. Teisseyre, T. Suski, M. Bockowski, S. Porowski, J. Domagala, C. Kirchner, A. Pelzmann, M. Schauler, M. Kamp, J. Cryst. Growth 198–199 (1999) 1061.
[89] K. Kumakura, T. Makimoto, N. Kobayashi, Japan J. Appl. Phys. 39 (2000) L337.
[90] T. Tanaka, A. Watanabe, H. Amano, Y. Kobayashi, I. Akasaki, S. Yamazaki, M. Koike, Appl. Phys. Lett. 65 (1994) 593.
[91] M. Suzuki, J. Nishio, M. Onomura, C. Hongo, J. Cryst. Growth 189–190 (1998) 511.
[92] J.B. Xia, K.W. Cheah, X.L. Wang, D.Z. Sun, M.Y. Kong, Phys. Rev. B 59 (1999) 10119.
[93] F. Mireles, S.E. Ulloa, Phys. Rev. B 58 (1998) 3879.
[94] P.-C. Chen, C.-H. Chen, S.-J. Chang, Y.-K. Su, P.-C. Chang, B.-R. Huang, Thin Solid Films 498 (2006) 113.
[95] T. Beierlein, S. Strite, A. Dommann, D.J. Smith, MRS Internet J. Nitride Semicond. Res. 2 (1997) 29.
[96] Y. Sato, A. Kurosaki, S. Sato, J. Cryst. Growth 189–190 (1998) 42.
[97] V. Bougrov, M. Levinshtein, S. Rumyantsev, A. Zubrilov, in: M.E. Levinshtein, S.L. Rumyantsev, M.S. Shur (Eds.), Properties of Advanced Semiconductor Materials: GaN, AlN, InN, BN, SiC, SiGe, John Wiley & Sons, Inc., New York, 2001 (Chapter 1).
[98] J. Wagner, A. Ramakrishnan, D. Behr, M. Maier, N. Herres, M. Kunzer, H. Obloh, K.-H. Bachem, MRS Internet J. Nitride Semicond. Res. 4S1 (1999) G2.8.
[99] X.Q. Shen, T. Ide, M. Shimizu, H. Okumura, J. Cryst. Growth 237–239 (2002) 1148.
[100] S. Nakamura, Diam. Relat. Mater. 5 (1996) 496.
[101] C.G. Van de Walle, M.D. McCluskey, C.P. Master, L.T. Romano, N.M. Johnson, Mater. Sci. Eng. B 59 (1999) 274.
[102] C. Wetzel, T. Takeuchi, S. Yamaguchi, H. Katoh, H. Amano, I. Akasaki, Appl. Phys. Lett. 73 (1998) 1994.
[103] M.D. McCluskey, C.G. Van de Walle, C.P. Master, L.T. Romano, N.M. Johnson, Appl. Phys. Lett. 72 (1998) 2725.
[104] Z. Dirdi, B. Bouhafs, P. Ruterana, Semicond. Sci. Technol. 18 (2003) 850.
[105] Y.-K. Kuo, W.-W. Lin, J. Lin, Japan J. Appl. Phys 40 (2001) 3157.
[106] M. Kurouchi, T. Araki, H. Naoi, T. Yamaguchi, A. Suzuki, Y. Nanishi, Phys. Status Solidi b 241 (2004) 2843.
[107] T. Takeuchi, H. Takeuchi, S. Sota, H. Sakai, H. Amano, I. Akasaki, Japan J. Appl. Phys. 36 (1997) L177.
[108] C.A. Parker, J. Roberts, S.M. Bedair, M.J. Reeds, S.X. Liu, N.A. El-Masry, L.H. Robins, Appl. Phys. Lett. 75 (1999) 2566.
[109] J. Wu, W. Walukiewicz, K.M. Yu, J.W. Ager III, E.E. Haller, H. Lu, W.J. Schaff, Phys. Status Solidi b 240 (2003) 412.
[110] W. Walukiewicz, S.X. Li, J. Wu, K.M. Yu, J.W. Ager III, E.E. Haller, H. Lu, W.J. Schaff, J. Cryst. Growth 269 (2004) 119.
[111] B.-T. Liou, S.-H. Yen, Y.-K. Kuo, Proc. SPIE 5628 (2005) 296.
[112] A.V. Voznyy, V.G. Deibuk, Semiconductors 38 (2004) 316.
[113] W. Shan, B.D. Little, J.J. Song, Z.C. Feng, M. Schurmann, R.A. Stall, Appl. Phys. Lett. 69 (1996) 3315.
[114] J. Wagner, A. Ramakrishnan, D. Behr, H. Obloh, M. Kunzer, K.-H. Bachem, Appl. Phys. Lett. 73 (1998) 1715.

[115] S. Chichibu, T. Azuhata, T. Sota, S. Nakamura, Appl. Phys. Lett. 70 (1997) 2822.
[116] S. Srinivasan, R. Liu, F. Bertram, F.A. Ponce, S. Tanaka, H. Omiya, Y. Nakagawa, Phys. Status Solidi b 228 (2001) 41.
[117] M. Schuster, P.O. Gervais, B. Jobs, W. Hossler, R. Averbeck, H. Riechert, A. Iberl, R. Stommer, J. Phys. D: Appl. Phys. 32 (1999) A56.
[118] K.P. O'Donnell, J.F.W. Mosselmans, R.W. Martin, S. Pereira, M.E. White, J. Phys.: Condens. Matter 13 (2001) 6977.
[119] S.Q. Zhou, M.F. Wu, L.N. Hou, S.D.H. Yao, J. Ma, R. Nie, Y.Z. Tong, Z.J. Yang, T.J. Yu, G.Y. Zhang, J. Cryst. Growth 263 (2004) 35.
[120] P.P.-T. Chen, K.S.A. Butcher, M. Winttrebert-Fouquet, R. Wuhrer, M.R. Philips, K.E. Prince, H. Timmers, S.K. Shrestha, B.F. Usher, J. Cryst. Growth 288 (2006) 241.
[121] Y. Ishitani, K. Xu, S.B. Che, H. Masuyama, W. Terashima, M. Yoshitani, N. Hashomoto, K. Akasaka, T. Ohkubo, A. Yoshikawa, Phys. Status Solidi b 241 (2004) 2849.
[122] V. Woods, N. Dietz, Mater. Sci. Eng. B 127 (2006) 239.
[123] D. Alexandrov, K.S.A. Butcher, T.L. Tansley, J. Cryst. Growth 288 (2006) 261.
[124] S.-H. Wei, X. Nie, I.G. Batyrev, S.B. Zhang, Phys. Rev. B 67 (2003) 165209.
[125] M.C. Johnson, S.L. Konsek, A. Zettl, E.D. Bourret-Courchesne, J. Cryst. Growth 272 (2004) 400.
[126] M. Wintrebert-Fouquet, K.S.A. Butcher, P.P.-T. Chen, J. Cryst. Growth 269 (2004) 134.
[127] B. Maleyre, S. Ruffenach, O. Briot, B. Gil, A. Van der Lee, Superlatt. Microstruct. 36 (2004) 517.
[128] G. Shikata, S. Hirano, T. Inoue, M. Orihara, Y. Hijikata, H. Yaguchi, S. Yoshida, J. Cryst. Growth 301–302 (2007) 517.
[129] X.D. Pu, J. Chen, W.Z. Shen, H. Ogawa, Q.X. Guo, J. Appl. Phys. 98 (2005) 033527.
[130] P.P. Chen, H. Makino, T.X. Li, J.B. Wang, W. Lu, T. Yao, Thin Solid Films 513 (2006) 166.
[131] T.L. Tansley, C.P. Foley, J. Appl. Phys. 59 (1986) 3241.
[132] W. Walukiewicz, S.X. Li, J. Wu, K.M. Yu, J.W. Ager III, E.E. Haller, H. Lu, W.J. Schaff, J. Cryst. Growth 269 (2004) 119.
[133] J.R. Jinschek, R. Erni, N.F. Gardner, A.Y. Kim, C. Kisielowski, Solid State Commun. 137 (2006) 230.
[134] R.W. Martin, P.G. Middleton, K.P. O'Donnell, W. Van der Stricht, Appl. Phys. Lett. 74 (1999) 263.
[135] I. Akasaki, H. Amano, Japan J. Appl. Phys. 36 (1997) 5393.
[136] J.W. Mathews, A.E. Blakeslee, J. Cryst. Growth 27 (1974) 118.
[137] A. Fischer, H. Kuhne, H. Richter, Phys. Rev. Lett. 73 (1994) 2712.
[138] P.F. Fewster, X-ray Scattering from Semiconductors, 2nd edition, Imperial College Press, London, 2003.
[139] S. Pereira, M.R. Correia, T. Monteiro, E. Pereira, E. Alves, A.D. Sequeira, N. Franco, Appl. Phys. Lett. 78 (2001) 2137.
[140] S. Pereira, M.R. Correia, T. Monteiro, E. Pereira, M.R. Soares, E. Alves, J. Cryst. Growth 230 (2001) 448.
[141] M.E. Vickers, M.J. Kappers, T.M. Smeeton, E.J. Thrush, J.S. Barnard, C.J. Humphreys, J. Appl. Phys. 94 (2003) 1565, and references quoted therein.
[142] S. Stepanov, W.N. Wang, B.S. Yavich, V. Bougrov, Y.T. Rebane, Y.G. Shreter, MRS Internet J. Nitride Semicond. Res. 6 (2001) 6.
[143] M. Yamaguchi, T. Yagi, T. Sota, T. Deguchi, K. Shimada, S. Nakamura, J. Appl. Phys. 85 (1999) 8502.
[144] S. Pereira, M.R. Correia, E. Pereira, K.P. O'Donnell, E. Alves, A.D. Sequeira, N. Franco, I.M. Watson, C.J. Deatcher, Appl. Phys. Lett. 80 (2002) 3913.
[145] A. Krost, J. Blasing, M. Junenburger, H. Protzmann, M. Heuken, Appl. Phys. Lett. 75 (1999) 689.
[146] E. Berkowiez, D. Gershoni, G. Bahir, E. Lakin, D. Shilo, E. Zolotoyabko, A.C. Abare, S.P. Denbaars, L.A. Coldren, Phy. Rev. B 61 (2000) 10994.
[147] H.H. Lee, H.W. Jang, D.H. Kim, D.Y. Noh, M.S. Yi, M. Tang, K.S. Liang, Physica B 336 (2003) 109.
[148] S. Pereira, M.R. Correia, E. Pereira, E. Alves, L.C. Alves, C. Trager-Cowan, K.P. O'Donnell, Mater. Res. Soc. Symp. Proc., vol. 639, b 3, 52.1, 2001.
[149] H. Angerer, D. Brunner, F. Freudenberg, O. Ambacher, M. Stutzmann, R. Hopler, T. Metzger, E. Born, G. Dollinger, A. Bergmaier, S. Karsch, H.-J. Korner, Appl. Phys. 71 (1997) 1504.
[150] Y. Narukawa, Y. Kawakami, S. Fujita, S. Fujita, S. Nakamura, Phys. Rev. B 55 (1997) R1938.
[151] S. Chichibu, T. Azuhata, T. Sota, S. Nakamura, Appl. Phys. Lett. 69 (1996) 4188.
[152] C. Kisielowski, Z. Liliental-Weber, S. Nakamura, Japan J. Appl. Phys. 36 (1997) 6932.
[153] P.G. Eliseev, P. Perlin, J. Lee, M. Osinki, Appl. Phys. Lett. 71 (1997) 569.
[154] K.P. O'Donnell, R.W. Martin, P.G. Middleton, Phy. Rev. Lett. 82 (1999) 237.
[155] T. Mukai, M. Yamada, S. Nakamura, Japan J. Appl. Phys. 37 (1998) 1358.

[156] T. Takeuchi, S. Sota, M. Katsuragawa, M. Komori, H. Takeuchi, H. Amano, I. Akasaki, Japan J. Appl. Phys. 36 (1997) 382.
[157] A. Hangleiter, J.S. Im, H. Kollmer, S. Heppel, J. Off, F. Scholz, MRS Internet J. Nitride Semicond. Res. 3 (1998) 15.
[158] P. Perlin, C. Kisielowski, V. Iota, B. Weinstein, L. Mattos, N.A. Shapiro, J. Kruger, E.R. Weber, J. Yang, Appl. Phys. Lett. 73 (1998) 2778.
[159] Y. Kawakami, K. Omae, A. Kaneta, K. Okamoto, Y. Narukawa, T. Mukai, S. Fujita, J. Phys.: Condens. Matter 13 (2001) 6993.
[160] A. Satake, Y. Masumoto, T. Miyajima, T. Asatsuma, F. Nakamura, M. Ikeda, Phys. Rev. B 57 (1998) R2041.
[161] H.J. Chang, C.H. Chen, Y.F. Chen, T.Y. Lin, L.C. Chen, K.H. Chen, Z.H. Lan, Appl. Phys. Lett. 86 (2005) 021911.
[162] M. Rao, D. Kim, S. Mahajan, Appl. Phys. Lett. 85 (2004) 1961.
[163] J. Zhou, G.-Y. Zhang, Chin. Phys. Lett. 19 (2002) 707.
[164] C. Kisielowski, Composition and strain fluctuations in InN/GaN/AlN heterostructures: A microscopic glimpse below surfaces, in: Proceedings of the 2nd International Symposium of Blue Laser and Light Emitting Diodes, Ohmsha Ltd., Chiba, Japan, 1998, pp. 321–326.
[165] F. Bernardini, V. Fiorentini, D. Vanderbilt, Phys. Rev. B 56 (1997) R10024.
[166] J.-S. Im, H. Kollmer, J. Off, A. Sohmer, F. Scholz, A. Hangleiter, Phys. Rev. B 57 (1998) R9435.
[167] M. Leroux, N. Grandjean, M. Laugt, J. Massies, B. Gil, P. Lefebvre, P. Bigenwald, Phys. Rev. B 58 (1998) R13371.
[168] B. Damilano, N. Grandjean, J. Massies, L. Siozade, L. Leymarie, Appl. Phys. Lett. 77 (2000) 1268.
[169] N.A. Shapiro, P. Perlin, C. Kieielowski, L.S. Mattos, J.W. Yang, E.R. Weber, MRS Internet J. Nitride Semicond. Res. 5 (2000) 1.
[170] T.J. Ochalski, B. Gil, P. Bigenwald, M. Bugajski, A. Wojcik, P. Lefebvre, T. Taliercio, N. Grandjean, J. Massies, Phys. Status Solidi b 288 (2001) 111.
[171] B. Monemar, J.P. Bergman, J. Dalfors, G. Pozina, B.E. Sernelius, P.O. Holtz, H. Amano, I. Akasaki, MRS Internet J. Nitride Semicond. Res. 4 (1999) 16.
[172] B. Monemar, Mater. Sci. Eng. B 59 (1999) 122.
[173] A. Koukitu, N. Takahashi, T. Taki, H. Seki, J. Cryst. Growth 170 (1997) 206.
[174] T. Saito, Y. Arakawa, Phys. Rev. B 60 (1999) 1701.
[175] T. Takeuchi, C. Wetzel, S. Yamaguchi, H. Sakai, H. Amano, I. Akasaki, Y. Kaneko, S. Nakagawa, Y. Yamaoka, N. Yamada, Appl. Phys. Lett. 73 (1998) 1691.